

Noninvasive optical imaging by speckle ensemble

Joseph Rosen and David Abookasis

Department of Electrical and Computer Engineering, Ben-Gurion University of the Negev, P.O. Box 653, Beer-Sheva 84105, Israel

Received June 2, 2003

We propose a new method imaging through scattering media. An object hidden between two biological tissues (chicken breast) is reconstructed from any speckled images obtained from the output of a multichannel optical imaging system. The effect of multiple imaging is achieved with a microlens array. Each lens in the array projects a different speckled image onto a digital camera. The set of speckled images from the entire array is first shifted to a common center and then accumulated into a single average picture. © 2004 Optical Society of America

OCIS codes: 030.6140, 030.6600, 170.1650, 170.3010, 170.3880.

In recent years much effort has been devoted to research in the optical imaging of objects embedded in a scattering medium. This topic has many potential applications. In medical diagnostics since it is safe, noninvasive, and relatively inexpensive compared with other often-used tomography techniques. Different optical imaging techniques have been proposed,¹ each of which has advantages and weaknesses.

The Earth's atmosphere is a well-investigated scattering medium. Stellar speckle interferometry, a method of imaging through the atmosphere, was invented more than 30 years ago by Labeyrie.² In this method, after many short-exposure photographs are collected, the square magnitude of the Fourier transform of each image is computed and accumulated to a single average power spectrum. However, the square magnitude lacks phase information, and in the end one can obtain only the average autocorrelation of the object function rather than its true shape.

In this Letter we propose a new scheme for imaging through a scattering medium. This scheme, inspired by stellar speckle interferometry, is termed noninvasive optical imaging by speckle ensemble (NOISE). It is based on a simple optical imaging system containing a microlens array (MLA) that images a hidden object through different parts of a scattering medium. We note that there is a space-time analogy between the temporal situation of Labeyrie's speckle interferometry and spatial NOISE. In the former, different speckled images are collected over time, with the atmospheric turbulence changing from one frame to another. On the other hand, in the case of NOISE the scattering medium is static. To collect different blurred images of the object through different scattering layers, the object should be observed from unrelated spatial parts of the same scattering medium. This goal is achieved by use of a MLA, with each lens in the array imaging from the same object through a different part of the scattering layer. However, unlike in the case of astronomical observation, we illuminate the embedded object from outside the medium with coherent light. Moreover, in our experiment we process the speckled patterns in the image plane rather than in the Fourier plane. Therefore the output result is an image of the object itself and not its autocorrelation. In this last sense astronomical observation, we illuminate the embedded object from outside the medium with coherent light.

Moreover, in our experiment we process the speckled patterns in the image plane rather than in the Fourier plane. Therefore the output result is an image of the object itself and not its autocorrelation. In this last sense, our method is closer to another speckle interferometry technique termed the shift-and-add algorithm.³ Other works related to our experiment deal with optical speckle tomography of biological tissues under ultrasound scanning.^{4,5} Since the ultrasound radiation modulates the optical speckle pattern, these technique provides dynamic analysis of speckle patterns.

In the experimental system, shown in Fig. 1, the object is illuminated from the back by a plane wave. Each individual lens in the array and spherical lens L operate in succession as two separate imaging systems. Without the scattering layers the coherently illuminated system is characterized by a relatively narrow point-spread function⁶ (PSF) $h_o(x, y)$. This PSF is calculated conventionally as an inverse Fourier transform of the aperture of a single microlens. In this case the microlens imposes the limit on the system bandwidth because its numerical aperture is smaller than that of lens L.

Next we consider the effect of backscattering layer S_1 . This layer diffuses the light such that each microlens receives almost the same amount of illumination. In addition, because of the randomness of medium S_1 and its uniformity, the object is multiplied by a random phase function with almost constant magnitude. Examples of such images are shown in Figs. 2(a) and 2(e) for the two objects used in our experiments. Up to this point, we could model the

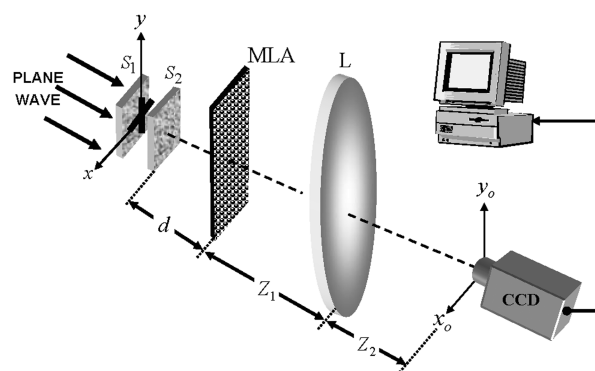


Fig. 1. Setup of the NOISE system.

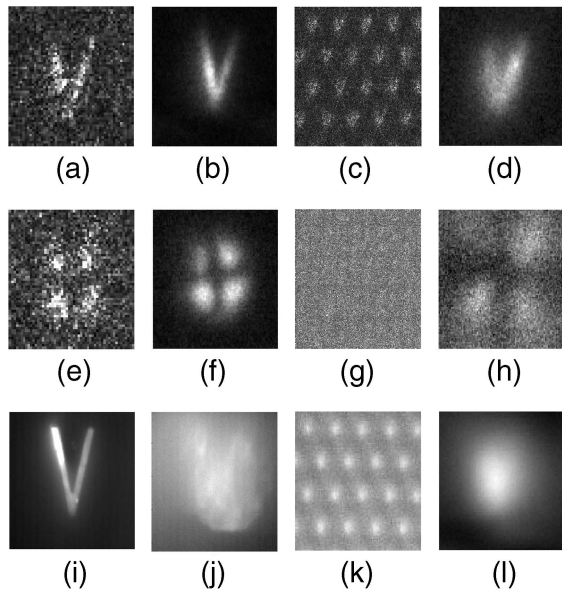


Fig. 2. (a) Image of the letter V in a single channel without layer S_2 . (b) Average picture of the entire array when the letter V is positioned in front of layer S_1 and layer S_2 is removed. (c) Several speckled pictures recorded by the CCD when the letter V was embedded between the two layers. (d) Final reconstructed result obtained from averaging 132 different imaging channels. (e)–(h) Same as (a)–(d) for the cross. (i) White-light image of the letter V in a single channel without layer S_2 . (j) White-light image of the letter V in a single channel, captured through layer S_2 . (k) Several pictures recorded by the CCD when the letter V was embedded between the two layers and illuminated by a broad white-light source. (l) Result obtained from averaging white-light images from 132 different channels.

entire system as an array of several identical imaging systems, all with the same PSF given by $h_o(\mathbf{r})$, where $\mathbf{r} = (x, y)$. Each imaging channel has an input function $t(\mathbf{r}) = A(\mathbf{r}) \cdot \exp[j\phi(\mathbf{r})]$, where $A(\mathbf{r})$ is the object amplitude function and $\phi(\mathbf{r})$ is a random phase function induced by layer S_1 . The image intensity at the k th coherently illuminated channel is given by⁶

$$I(\mathbf{r}_o) = |t(\mathbf{r}_o) * h_o(\mathbf{r}_o)|^2, \quad (1)$$

where the asterisk denotes two-dimensional convolution and $\mathbf{r}_o = (x_o, y_o)$. $I(\mathbf{r}_o)$ of Eq. (1) is the diffraction-limited image of the squared function of the object, $|A(\mathbf{r}_o)|^2$. The goal of the following proposed procedure is to produce an intensity distribution that is as close as possible to $I(\mathbf{r}_o)$.

When the front scattering layer S_2 is introduced into the system, the output image is distorted such that the object cannot be recognized. Since each microlens observes the object through a different transverse cross section of the scattering layer, each k th microlens, together with lens L, creates a linear system characterized by a different random PSF $h_k(\mathbf{r})$. Therefore the output intensity pattern in each coherently illuminated k th channel is given by $\tilde{I}_k(\mathbf{r}_o) = |t(\mathbf{r}_o) * h_k(\mathbf{r}_o)|^2$. It is assumed that, although each PSF $h_k(\mathbf{r})$ is a random

function that is wider than $h_o(\mathbf{r})$, the ensemble average PSF over all K channels satisfies the relation

$$\frac{1}{K} \sum_k h_k(\mathbf{r}) \equiv h_o(\mathbf{r}). \quad (2)$$

Having the set of K speckled images $\{\tilde{I}_k(\mathbf{r}_o)\}$, we first center each one of them and then sum them to a single average image given by

$$S(\mathbf{r}_o) = \frac{1}{K} \sum_k |t(\mathbf{r}_o) * h_k(\mathbf{r}_o)|^2. \quad (3)$$

To show that this ensemble average is approximately equal to the diffraction-limited image given by Eq. (1), the convolution of Eq. (3) is explicitly written, and the order of integration and summation is interchanged as follows:

$$S(\mathbf{r}_o) = \int_{-\infty}^{\infty} \int_{-\infty}^{\infty} t(\mathbf{r}_1) t^*(\mathbf{r}_2) \left[\frac{1}{K} \sum_k h_k(\mathbf{r}_o - \mathbf{r}_1) \times h_k^*(\mathbf{r}_o - \mathbf{r}_2) \right] d\mathbf{r}_1 d\mathbf{r}_2, \quad (4)$$

where the superscript asterisk denotes the complex conjugate. The internal averaging in Eq. (4) can be separated into two summations, one includes all the pairs of functions $h_k(\mathbf{r})$ shifted by different distances, i.e., $\mathbf{r}_1 \neq \mathbf{r}_2$. The ensemble average in this case is calculated by the multiplication of two uncorrelated random variables, and hence this ensemble average is equal to the multiplication of their ensemble averages. The second summation represents all the pairs of function shifted equally, i.e., $\mathbf{r}_1 = \mathbf{r}_2$. This latter sum is the ensemble average on the set of random functions $\{|h_k(\mathbf{r})|^2\}$, which based on Eq. (2) is given by $\frac{1}{K} \sum_k |h_k(\mathbf{r})|^2 \equiv |h_o(\mathbf{r})|^2 + \sigma^2(\mathbf{r})$, where σ^2 is the variance of the random set $\{h_k(\mathbf{r})\}$ and is defined as $\sigma^2(\mathbf{r}) = \frac{1}{K} \sum_k |h_k(\mathbf{r}) - h_o(\mathbf{r})|^2$. Under the assumption of a weak scatterer, we assume that this variance along \mathbf{r} is much smaller than $\max_{\mathbf{r}} |h_o(\mathbf{r})|^2$, but it is not negligible. Based on the above arguments, Eq. (4) becomes

$$S(\mathbf{r}_o) \equiv |t(\mathbf{r}_o) * h_o(\mathbf{r}_o)|^2 + |t(\mathbf{r}_o)|^2 * \sigma^2(\mathbf{r}_o). \quad (5)$$

The first term of Eq. (5) is the desired diffraction-limited image given by Eq. (1). The second term is a convolution between the object and the variance functions. Clearly $\sigma^2(\mathbf{r})$ is wider than $h_o(\mathbf{r})$ because the scattering layer broadens the diffraction-limited image of a point. Therefore we conclude that the second convolution in Eq. (5) blurs the diffraction-limited image of the object. The value of this blurring term is determined by the average value of the variance $\sigma^2(\mathbf{r})$. The contrast and the sharpness of the reconstructed object are inversely dependent on the variance.

To demonstrate the proposed technique, two binary objects were separately embedded between two layers of chicken breast separated from each other by a distance of 12 mm. One is a transparent object in the form of the letter V that measures 7 mm \times 11 mm, and the other is an opaque object in the form of a cross that measures 9 mm \times 9 mm. Figure 2(b) and 2(f) are the

average pictures of the entire array when only layer S_1 exists in the setup and S_2 is removed. The thickness of rear tissue S_1 was approximately 3 mm in both experiments, whereas the thickness of front tissue S_2 was approximately 4 mm for the letter V and 8 mm for the cross. A reduced scattering coefficient of the tissues of $\mu'_s = 4.5 \pm 0.3 \text{ cm}^{-1}$ was measured by the method proposed in Ref. 7. Assuming the anisotropy factor⁸ is $g = 0.965$, the scattering coefficient becomes $\mu_s = \mu'_s / (1 - g) = 128 \pm 9 \text{ cm}^{-1}$. Rear tissue S_1 was illuminated by a collimated plane wave from a He-Ne laser of $\lambda = 633 \text{ nm}$. The MLA, placed a distance of $d = 155 \text{ mm}$ from S_2 , is composed of 115×100 hexagonal refractive lenses, but only the central 132 (12×11) lenses are used in these experiments. The radius of each microlens is $r_l = 250 \mu\text{m}$, and their focal length is 3.3 mm. Under these conditions the optical system without the tissues can resolve a minimum size of $\lambda d / r_l \approx 0.4 \text{ mm}$. The image plane of the MLA is projected onto the CCD plane by a single spherical lens L, with a 300-mm focal length. Distances Z_1 and Z_2 shown in Fig. 1 are 520 and 710 mm, respectively. In the experiment we used a digital CCD camera that measured 1280 pixels horizontally and 1024 pixels vertically within an $8.6 \times 6.9 \text{ mm}$ active area.

The original object cannot be recognized from any image of the 132 different blurred images, several of which are shown in Fig. 2(c) for the letter V and in Fig. 2(g) for the cross. Each blurred subimage of 96×84 pixels from the array was extracted from the matrix and shifted toward a common center. We used two different strategies to center the blurred images, and both operated with success. One method was to calculate the center of gravity of each blurred cloud of the entire set of 132 blurred images. The center of gravity is considered the true center of the object in each frame, and accordingly all the images are centered to have the same center of gravity. In the second method we calibrated in advance all the shifts needed in each picture by observing an object without front scattering layer S_2 . The suitable shifts are those that led to a maximum overlap between all the images. The reconstruction results are shown in Fig. 2(d) for the letter V and in Fig. 2(h) for the cross. The original objects are recognized in both examples. The blurring of the original object predicted by Eq. (5) can also be seen clearly.

To verify that it is necessary to use coherent light, we imaged through the same scattering layer with incoherent light. Figure 2(i) shows the image obtained without front layer S_2 under white-light illumination from a halogen lamp. When front layer S_2 is introduced into the system, the picture obtained in each channel is a wide blurry spot as shown in Fig. 2(j). In this case the thickness of the rear slice is 3.5 mm and that of the front slice is 4 mm. All the pictures of the set seem to be more or less the same wide smoothly blurry spots shown in Fig. 2(k). Averaging over all 132 pictures yields the result shown in Fig. 2(l). The letter V cannot be recognized from Fig. 2(l). Incoherent light means that the object is illuminated by a large number of plane waves with many different an-

gles. The effect on the output image in each channel is an accumulation of many blurred images of the object shifted randomly from the true object center. Therefore the result in each imaging channel is a smoothly blurred unrecognizable image of the object. Accumulating these images along all the channels does not allow us to see through the scattering medium. Illuminating the medium with a broad spectral pointlike source, such as a superluminescent diode, may also yield a smooth blurred image in each channel due to dispersion resulting from the scattering layer. However, this prediction should be verified experimentally in the future.

In another experiment we removed the MLA and imaged the object onto the CCD with a resolution that was 48 times better than that in the setup with the MLA. Then every successive rectangle of 48×48 pixels on the image matrix was averaged. The aim of this experiment was to verify that lateral averaging over a high-resolution image is not equivalent to averaging over many low-resolution images, as done in the experiment with the MLA. These results did not produce any recognizable image of the object. This shows that the procedure of averaging the low-resolution MLA images is significantly superior to averaging a single high-resolution image.

In conclusion, by the NOISE technique we have been able to reconstruct the shape of binary objects embedded between two scattering layers. The weakness of the setup is the relatively low spatial bandwidth product of the diffraction-limited system. The use of a small aperture lens at each imaging channel reduces both the field of view and the system's bandwidth. However, this drawback seems a reasonable price to pay for the ability to image through a scattering medium in a simple and robust way. The advantages of the method are relative simplicity, low cost, fast operation, and the need for only low-power cw laser illumination. Because of all these advantages, NOISE might be useful for many imaging applications, especially in medical diagnostics.

This research was supported by the Israel Science Foundation. J. Rosen's e-mail address is rosen@ee.bgu.ac.il.

References

1. J. C. Hebden, S. R. Arridge, and D. T. Delpy, *Phys. Med. Biol.* **42**, 825 (1997).
2. A. Labeyrie, *Astron. Astrophys.* **6**, 85 (1970).
3. R. H. T. Bates and F. M. Caddy, *Opt. Commun.* **32**, 365 (1980).
4. S. Lévêque, A. C. Boccara, M. Lebec, and H. Saint-Jalmes, *Opt. Lett.* **24**, 181 (1999).
5. J. Li, G. Ku, and L. H. V. Wang, *Appl. Opt.* **41**, 6030 (2002).
6. J. W. Goodman, *Introduction to Fourier Optics*, 2nd ed. (McGraw-Hill, New York, 1996), Chap. 6, pp. 126–130.
7. L. Wang and S. L. Jacques, *Appl. Opt.* **34**, 2362 (1995).
8. W.-F. Cheong, S. A. Pahl, and A. J. Welch, *IEEE J. Quantum Electron.* **26**, 2166 (1990).